

Contents lists available at ScienceDirect

Renewable Energy

journal homepage: www.elsevier.com/locate/renene



Numerical modeling of homogeneous gas and heterogeneous char combustion for a wood-fired hydronic heater



Joseph P. Richter, Joshua M. Weisberger, Brian T. Bojko, Joseph C. Mollendorf, Paul E. DesJardin*

Department of Mechanical and Aerospace Engineering, University at Buffalo, the State University of New York Buffalo, NY 14260-4400, USA

ARTICLE INFO

Article history:
Received 28 March 2018
Received in revised form
13 July 2018
Accepted 18 July 2018
Available online 23 July 2018

Keywords: Biomass combustion Hydronic heater Variable fuel Emissions

ABSTRACT

The pyrolysis of woody fuels produces two main products - pyrolysis gases and solid residue char which undergo homogeneous and heterogeneous reactions, respectively. Recent experimental measurements using a two-stage hydronic heater indicate the oxidization of these two products occur at distinctly different time scales with the pyrolysis gases burning immediately, and the majority of the char oxidization occurring later. In this study, these two oxidation pathways are explicitly accounted for in a numerical model that considers a non-homogeneous mixture of product flue gases. The model is based on a three-zone description of the heater which accounts for combustion and heat transfer using well-stirred reactor theory. The first zone describes the gasification of the wood fuel and burning of both pyrolysis gases and char. The second zone represents an after-burning stage. The last stage accounts for the transport of gases out the flue. Model predictions of O_2 , CO_2 , CO_3 , CO_4 , CO_3 , CO_4 , CO_4 , and temperature are compared to experimental measurements showing good overall agreement. Furthermore, the dual oxidation pathway description of combustion is shown to be critical to account for the dual-peak CO_4 time signature. The first peak is associated with the burning of pyrolysis gases and the second corresponds to char oxidation.

© 2018 Elsevier Ltd. All rights reserved.

1. Introduction

Biomass is expected to account for up to 30% of the world's annual demand for energy by 2050 [1]. With this growing need for energy, one of the prevailing challenges in using biomass combustion systems is reducing harmful emissions. For the northeastern US, emissions from wood fired heaters is one of the leading sources of reduced air quality. To provide stricter guidelines on the certification of these systems, the Environmental Protection Agency (EPA) has recently defined new regulations for wood burning appliances (which include wood stoves, masonry heaters, pelletburning stoves and hydronic heaters) [2]. Therefore, with the aim to better understand and reduce pollution, many studies focus on the characterization of emissions from specific domestic and commercial biomass energy systems [3,4].

A review of biomass hydronic heaters by Saidur et al. [5] groups appliances into pellet [6,7], wood chips [8,9], cord-wood [10], wood

* Corresponding author. E-mail address: ped3@buffalo.edu (P.E. Des|ardin). briquettes [11], and coal [12] based systems. For pellet and wood chip (small particle) feed systems, the fuel flow rate is predictable and controlled, allowing for quasi-steady-state operation. Consequently, emissions are better understood and optimized. Less is known about cord-wood (large particle) systems since they typically burn as an unsteady batch process. Complex computational models are often used to help in the development and design of biomass appliances since they provide spatially and temporally resolved simulations, however they are often computationally expensive to run even under steady state conditions [3,6,7,12]. A study by Persson et al. [13] uses the transient systems simulation package TRNSYS to develop an energy model for a wood pellet boiler. The TRNSYS based model shows overall agreement with system measurements, but found that improvement with regard to the dynamic response in relation to the large thermal inertia of the water is required. Alternatively, a more basic system level approach has been studied for downdraft gasifiers for generating "producer gas" [14,15], with good agreement with measurements. However for large particle unsteady batch-run systems of domestic wood boilers, modeling can be particularly challenging with few studies published [16]. Often there exist multiple unpredictable systemic

Nomenclature		σ	Stefan-Boltzmann constant [W/m^2-K^4]
h	heat transfer coefficient [W/m 2 – K]	Subscripts/Superscripts	
h_i	enthalpy [MJ/kg]	1	primary chamber/zone
Δh	heat [MJ/kg]	2	secondary chamber/zone
m	mass [kg]	3	flue chamber/zone
m	mass flow rate [kg/hr]	air	air
t	time [hr]	b	boiler
Α	area [m²]	char	char
C	heat capacity $[J/kg - K]$	del	delivered
G	Gibbs free energy [k]/kg]	gas	gas
Н	enthalpy [kJ/kg]	g-b	gas to boiler
L	latent heat [MJ/kg]	H_2O	water
Q	heat [/]	i	i th species
Q	heat rate [W]	in	in
S	entropy [k]/K]	n	n th term
T	temperature [K]	0	initial
Y	species mass fraction	out	out
Z	mixture fraction	prod	products of combustion
_		pyr	pyrolysis
Greek		S	steel
ρ	density [kg/m ³]	tot	total
ϕ	equivalence ratio	wood	wood

factors which contribute to model uncertainties [17–19]. Accurate representation of emissions is particularly difficult in batch-run systems due to the nature of non-homogeneous biomass decomposition and coupling of homogeneous combustion of the gases with the heterogeneous oxidation of the char.

In this study, a system level model is developed for a two stage wood fired boiler containing two combustion chambers. The first is associated primarily with wood pyrolysis while the second, located downstream, is designed for secondary burning of undesirable emissions. A photograph of the hydronic heater/boiler is shown in Fig. 1 (a) with the upper and lower chamber doors identified. The

internal layout of the boiler can be seen in Fig. 1(b) where the gas flow path and primary and secondary (blower) air can be seen. During a typical burn, the solid wood fuel undergoes an unsteady decomposition where Fig. 2 shows the wood combustion in the primary chamber during early time compared to that in later time. Early in the burn evolution the virgin wood undergoes pyrolysis where homogeneous combustion of the off-gases produce large flames. As the run progresses, more char (solid carbon) remains, leaving minimal flames and transitions more towards heterogeneous char oxidation. This observation is the motivation for this study in two respects. First, since the fuel is changing over time, a

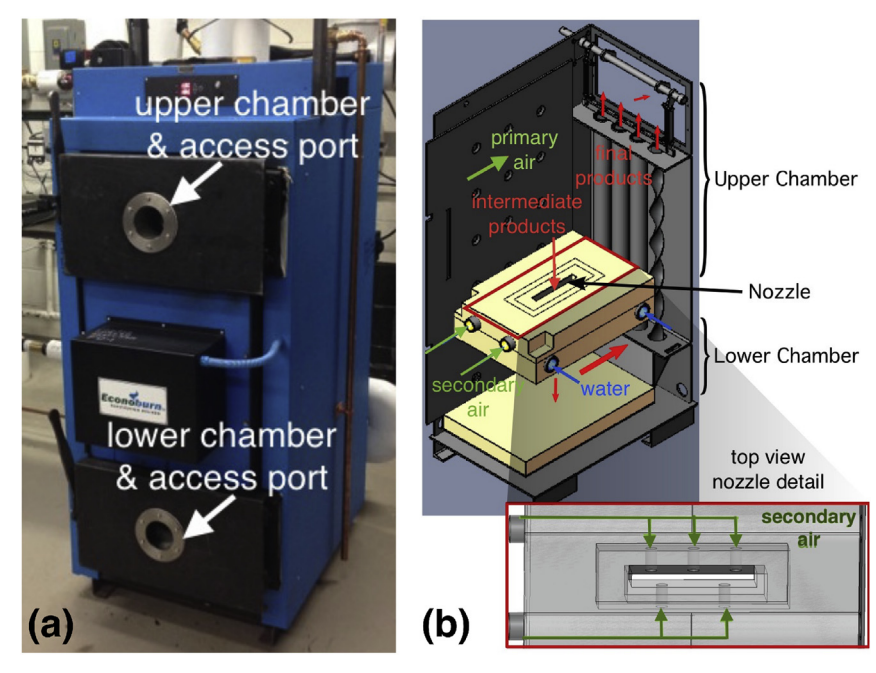


Fig. 1. (a) Picture of Econoburn Boiler EBW-200 and (b) internal cross-sectional view of boiler.



Fig. 2. Pictures of fuel burn during early and late time.

constant fuel composition is not a physically realistic assumption. Second, there is both homogeneous combustion of the gases and heterogeneous oxidation of the char which operate within distinctly separate time scales, requiring the need for dual oxidation pathways.

The rest of this study is organized as follows. In Section 2 the numerical model formulation for the three zone system will be discussed. Section 3 will provide details on the pyrolysis and combustion models. The experimental setup will be discussed in Section 4. Results will be presented in Section 5 and conclusions are drawn in Section 6.

2. Numerical model formulation

This study builds on the single chamber model developed by Richter et al. 2016 [16]. In this study we use energy conservation equations derived individually for three separate "zones" in the boiler, each with (steel + water = b), gas (g), and wood fuel (wood). The three zones are segmented into a gas and boiler control volume as shown in Fig. 3. The subscript numeral (1,2 and 3) indicates the associated zone ascribed for that variable and the letter "k" is used as a general marker representing any of the zones. The conservation equations for the primary chamber are as follows

$$m_{g1}C_{g1}\frac{dT_{g1}}{dt} = \dot{m}_{wood} \sum_{i_{wood}} Y_{i,pyr} h_{i,pyr} (T_{pyr}) - \dot{Q}_{g1-b1} + \dot{Q}_{air1} - \dot{Q}_{prod1} + \dot{m}_{wood} L_{pyr}$$
(1)

$$m_{b1}C_{b1}\frac{dT_{b1}}{dt} = \dot{Q}_{g1-b1} - \dot{Q}_{del1}$$
 (2)

where

$$\dot{Q}_{del1} = (A_{b1}/A_{tot})C_{H_2O}\dot{m}_{H_2O}(T_{H_2O,out} - T_{H_2O,in})$$
(3)

is the heat delivered to the thermal load (heat exchanger) which is experimentally determined from measurements of the water temperature and flow rate going in $(T_{H_2O,in})$ and out $(T_{H_2O,out})$ of the boiler, and segmented for each respective chamber (k) based on chamber surface area ratios where A_{bk} represents the internal wetted surface area of zone k and A_{tot} is the total internal wetted surface area. For example, the delivered heat rate from the subsequent zones would be generally defined as;

$$\dot{Q}_{delk} = (A_{bk}/A_{tot})C_{H_2O}\dot{m}_{H_2O}(T_{H_2O,out} - T_{H_2O,in})$$
(4)

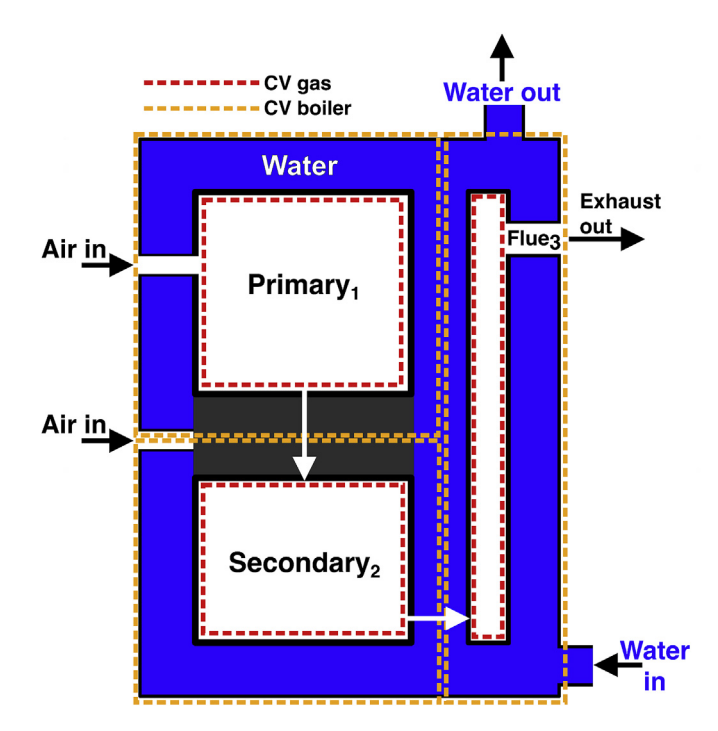


Fig. 3. Outline of Boiler zones showing control volumes used in model, where subscripts indicate associated zone.

The quantity \dot{Q}_{g1-b1} represent the energy transfer rate from the gas to the boiler in zone 1. The heat transfer from the gas to the boiler is modeled using a mixed convective and radiative condition assuming black surfaces;

$$\dot{Q}_{g1-b1} = A_{g1-b1} \left[h_{g1-b1} (T_{g1} - T_{b1}) + \sigma \left(T_{g1}^4 - T_{b1}^4 \right) \right]$$
 (5)

where h_{g1-b1} is the heat transfer coefficient across the gas-boiler interface with internal gas wetted area A_{b1} , and $\sigma = 5.567 \times 10^{-8} \text{W/m}^2 - \text{K}^4$ is the Stefan-Boltzmann constant. Since the thermal inertia of the wood fuel is small relative to that of the boiler, the wood is assumed to be at its pyrolysis temperature, i.e. $dT_{wood}/dt \approx 0$, where the heat transfer from the wood to the gas can be defined $\dot{Q}_{wood-g1} = \dot{m}_{wood}L_{pyr}$. In Eq. (1), L_{pyr} is the latent heat of pyrolysis and \dot{m}_{wood} is the total fuel mass loss rate of the wood which is experimentally measured using a load cell [16]. Ash in oak is typically less than 0.5% by mass of the dry fuel [20], and is

ignored in this analysis. The fuel species are defined where $Y_{i,pyr}$ are the mass fractions of the pyrolysis gases and $h_{i,pyr}$ is the enthalpy of the i^{th} species at the wood pyrolysis temperature, T_{pyr} . The energy flow of air in and products out of the primary chamber are defined as;

$$\dot{Q}_{air1} = \dot{m}_{air1} h_{air1} \tag{6}$$

$$\dot{Q}_{prod1} = \dot{m}_{prod1} \sum_{i_{g1}} Y_{i,g1} h_{i,g1} (T_{g1})$$
 (7)

where \dot{m}_{prod1} is the total exhaust gas flow rate for the primary zone defined as: $\dot{m}_{prod1} = \dot{m}_{air1} + \dot{m}_{wood}$, for the secondary zone $\dot{m}_{prod2} = \dot{m}_{air2} + \dot{m}_{prod1}$, and for the flue $\dot{m}_{prod3} = \dot{m}_{prod2}$ where no additional air is introduced. Incoming blower air flow rates in the primary and secondary chamber respectively are defined as $\dot{m}_{air1} = 0.6 \, \dot{m}_{total}$ and $\dot{m}_{air2} = 0.4 \, \dot{m}_{total}$ where the separation ratios are set manually through internal flow dampeners.

The gas control volume conservation is modified to account for separate pyrolysis gas (gas) and char (char), so the fuel enthalpy may be expressed as,

$$\begin{split} \dot{m}_{wood} \sum_{i_{wood}} & Y_{i,pyr} h_{i,pyr} \left(T_{pyr} \right) = \dot{m}_{gas} \sum_{i_{gas}} & Y_{i,gas} h_{i,gas} \left(T_{gas} \right) \\ & + \dot{m}_{char} \sum_{i_{char}} & Y_{i,char} h_{i,char} \left(T_{char} \right) \end{split} \tag{8}$$

and the associated air used for oxidation is also split into two streams,

$$\dot{Q}_{air1} = \dot{Q}_{air1,gas} + \dot{Q}_{air1,char} \tag{9}$$

resulting in separate product streams which are used to feed the secondary chamber.

$$\dot{Q}_{prod1} = \dot{Q}_{prod1,gas} + \dot{Q}_{prod1,char} \tag{10}$$

The energy conservation equations for the secondary after burning zone are,

$$\begin{split} m_{g2} C_{g2} \frac{dT_{g2}}{dt} &= \dot{m}_{prod1} \sum_{i_{prod1}} Y_{i,prod1} h_{i,prod1} \left(T_{g1} \right) - \dot{Q}_{g2-b2} + \dot{Q}_{air2} \\ &- \dot{Q}_{prod2} \end{split} \tag{11}$$

$$m_{b2}C_{b2}\frac{dT_{b2}}{dt} = \dot{Q}_{g2-b2} - \dot{Q}_{del2}$$
 (12)

where the energy flow of air into the secondary chamber is defined as $\dot{Q}_{air2} = \dot{m}_{air2} h_{air2}$. The separation of the fuel stream for the secondary chamber is handled with a few differences. First the secondary air stream is fully mixed with the pyrolysis gas products from the primary chamber, the char products are assumed chemically frozen but allowed to reach thermal equilibrium with the other products. The secondary chamber fuel energy flow is therefore expressed as;

$$\dot{m}_{prod1} \sum_{i_{prod1},gas} Y_{i,prod1} h_{i,prod1} \left(T_{g1} \right) = \dot{m}_{prod1,gas}$$

$$\sum_{i_{prod1},gas} Y_{i,prod1,gas} h_{i,prod1,gas} \left(T_{g1} \right) + \dot{m}_{prod1,char}$$

$$\sum_{i_{prod1,char}} Y_{i,prod1,char} h_{i,prod1,char} \left(T_{g1} \right)$$
(13)

$$\dot{Q}_{prod2} = \dot{Q}_{prod2,gas} + \dot{Q}_{prod2,char} \tag{14}$$

The third chamber is the flue zone where no additional air is introduced and all reactants are assumed chemically frozen. The conservation equations are defined below.

$$m_{g3}C_{g3}\frac{dT_{g3}}{dt} = \dot{m}_{prod2}\sum_{i_{prod2}}Y_{i,prod2}h_{i,prod2}(T_{g2}) - \dot{Q}_{g3-b3} - \dot{Q}_{prod3}$$
(15)

$$m_{b3}C_{b3}\frac{dT_{b3}}{dt} = \dot{Q}_{g3-b3} - \dot{Q}_{del3}$$
 (16)

The overall numerical model is driven by two experimental inputs, \dot{m}_{wood} and \dot{Q}_{del} . The measurement of those two inputs is discussed further in Section 4. Equations (1), (2), (11), (12), (15) and (16) are integrated in time using a semi-implicit time marching scheme. In this approach, temperature time derivatives are disusing first-order forward differences, $dT/dt \simeq (T^{n+1} - T^n)/\Delta t$ and all source term quantities on the right hand side are evaluated at the n + 1 time level. The system of nonlinear algebraic equations are solved using an algorithm that employs Brent's method, where convergence is defined when changes in T_{nk}^{n+1} are smaller than a specified error tolerance [21]. For each iteration, the chemical composition of the chamber gases and temperature T_{gk}^{n+1} are updated until convergence is achieved for that time step. Input parameters for the model are summarized in Table 1.

Summary of parameters for system level model

Parameter	Value	
m_b	1054 kg	
$m_{\rm s}$	898 kg	
m_{H_2O}	155 kg	
m_{wood}	28 kg	
L _{pyr}	6.73 MJ/kg	
h_{gb1}	$50 \text{ W/m}^2 \cdot \text{K}$	
h_{gb2}	$360 \text{W/m}^2 \cdot \text{K}$	
h_{gb3}	$24 - 26 \text{ W/m}^2 \cdot \text{K}[42]$	
T_{pyr}	700 K	
Moisture content	8.3%	
A_{wood}	0.504 m^2	
A _{tot}	4.1 m ²	
A_{b1}	2.07 m ²	
A_{b2}	1.21 m ²	
A_{b3}	0.82 m^2	
$ ho_{wood}$	1150 kg/m^3	
C_{wood}	1360 J/kg·K	
C_b	1037 J/kg⋅K	
C _s	490 J/kg·K	
C_{H_2O}	4188 J/kg·K	

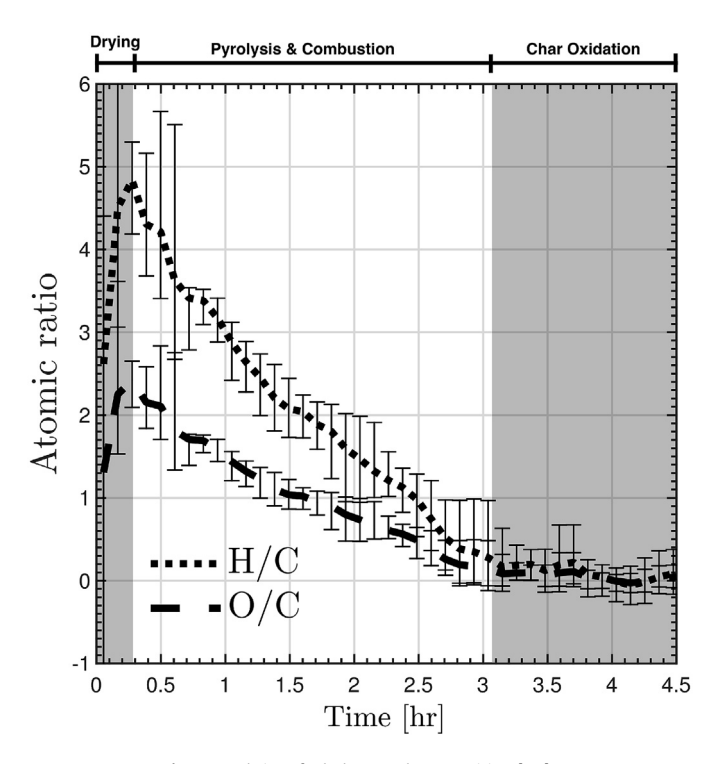


Fig. 4. Real time fuel elemental composition [22].

3. Pyrolysis and combustion models

3.1. Pyrolysis model

One of the challenges in modeling the emissions in biomass fired systems is in accurately defining the incoming fuel composition. This difficulty is primarily why many biomass modeling efforts focus on steady state systems with small particle fuels (i.e., pellets. wood chips, etc.) which can be assumed to be approximately constant. A recent study by Richter et al. 2016 [22], shows that changes in larger fuels (i.e., cordwood, BIOBLOCKS®, etc.) composition can be considerably large. Distinct stages of drying, pyrolysis/combustion and charcoal oxidation can be identified from inferred H/C and O/C atomic ratios of the fuel shown in Fig. 4. In the drying stage, the majority of unbound fuel moisture has been driven from the fuel, resulting in an increase in H/C atomic ratio of the fuel. This is further supported by integrating the fuel based H_2O where approximately 2.2 kg (amount of free H_2O contained in 28 kg of 8.3% moist fuel) has been released at approximately 0.25 h, corresponding with the end of the drying stage. The second stage consists of a combination of virgin fuel pyrolysis and combustion resulting in a linear decrease in H and O with time until the fuel H has been oxidized. Stage three, starting at approximately 2.75 h, is characterized by the full consumption of H and O leading to the

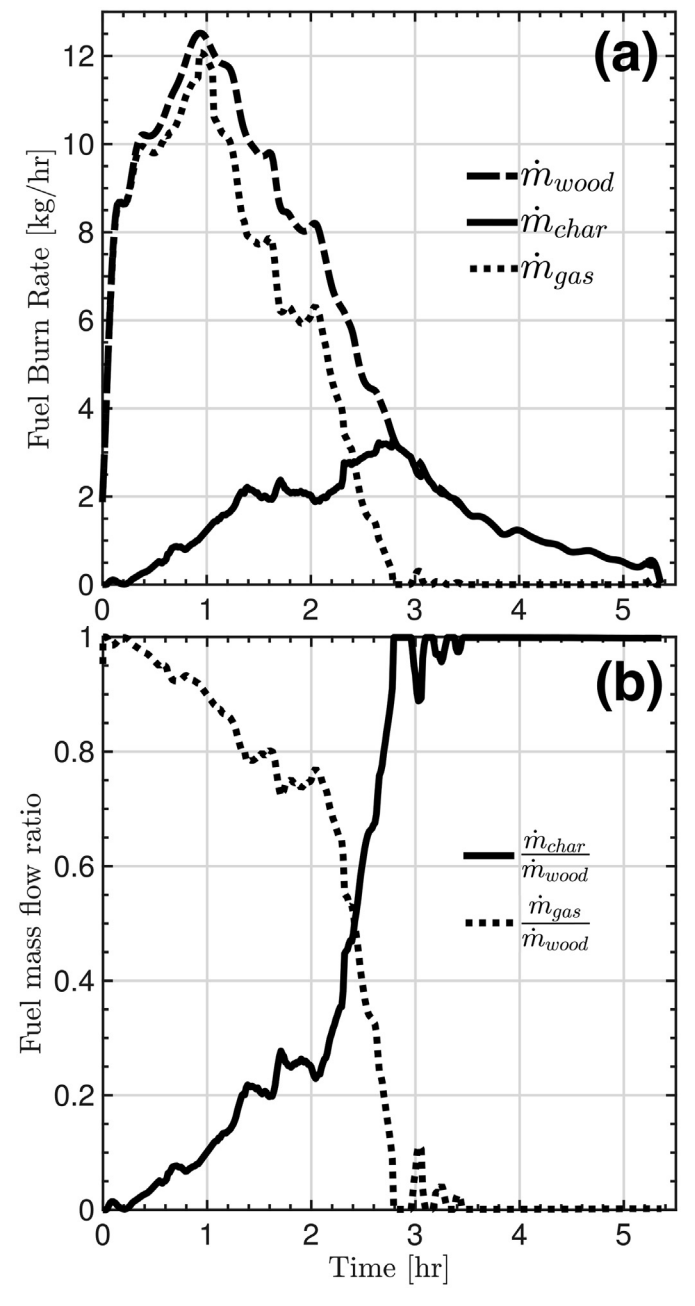


Fig. 6. Fuel burn rate versus time for (a) char, gas and total wood fuel streams and (b) mass flow rate of char and gas normalized by the total wood burn rate.

charcoal oxidation stage.

While complex charring pyrolysis models are available to define the gases generated from thermal decomposition of the biomass fuel [23], they often involve layers of assumptions to achieve a

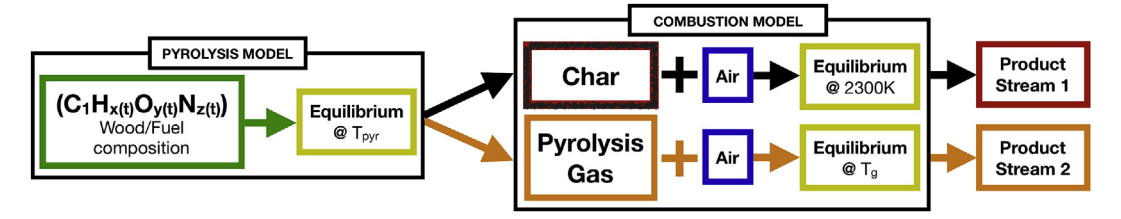


Fig. 5. Flowchart showing pyrolysis model and fuel oxidation pathways in the primary chamber.

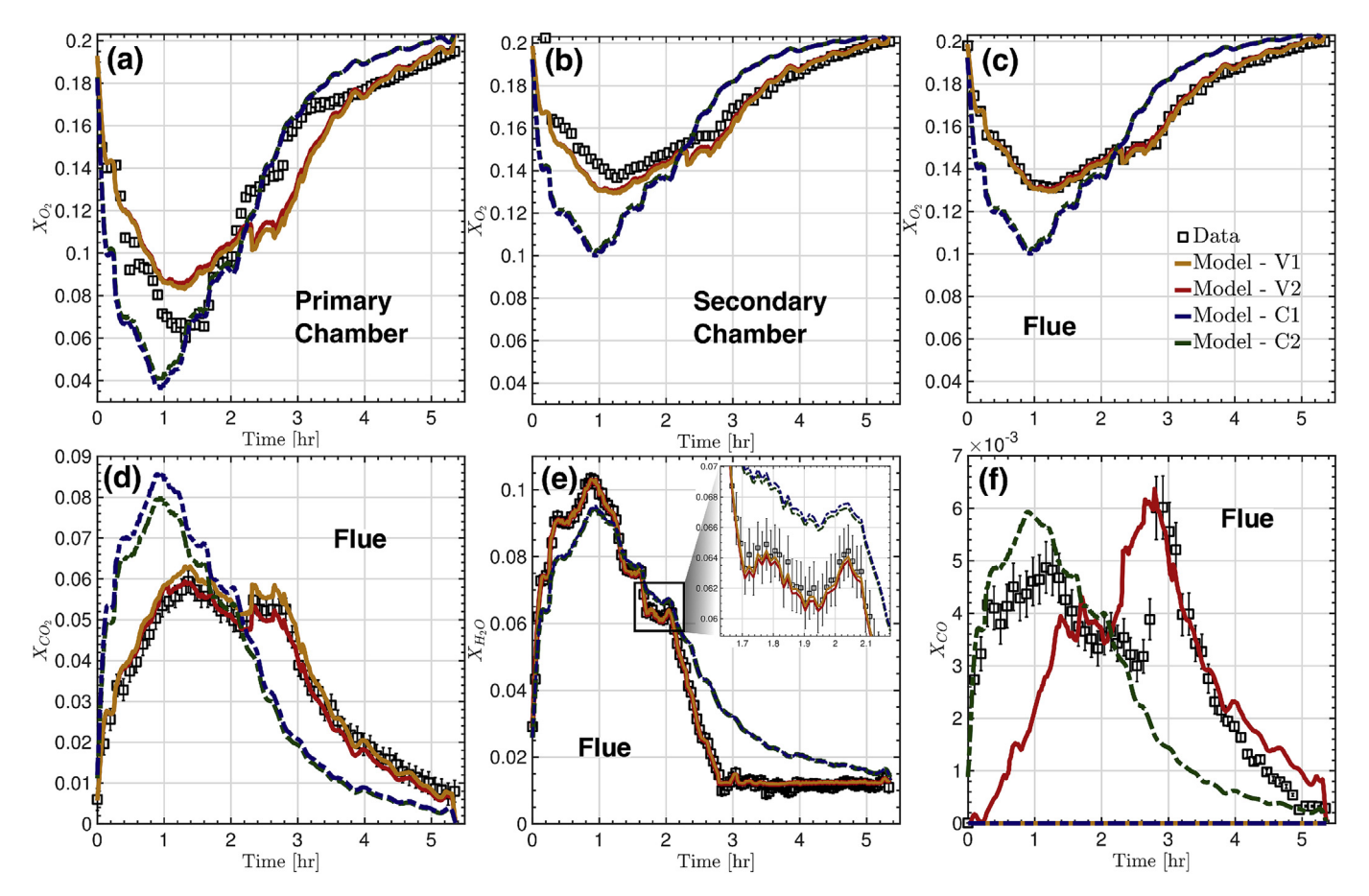


Fig. 7. Comparison of experimental data and model calculations for time dependent emissions concentrations for O_2 , CO_2 , H_2O and CO for several cases including model results run with variable or constant fuel composition (V or C) and single or dual (1 or 2) oxidation pathways.

tractable solution (e.g., temperature equilibrium, equal strains, etc.) [24–27]. In this study an experimentally derived fuel decomposition model is developed from measurements of flue exhaust species described in Refs. [22] and [10]. This time varying elemental fuel composition is used to define a mixture of pyrolysis gases consisting of (CH_4 , O_2 , CO, NO, H_2O , CO_2 , N_2 , C_3H_8 , H_2 , OH and C(s)) and assuming two-phase chemical equilibrium at fixed pyrolysis temperature $T_{pyr} = 425^{\circ}\text{C}$ (700 K), consistent with reported pyrolysis temperatures [28,29].

The open-source chemical kinetics software, Cantera, is used to solve the multiphase chemical equilibrium composition using a Villars-Cruise-Smith minimization algorithm [30–33]. As shown in Fig. 5, the pyrolysis gases and solid char are then treated separately with regard to oxidation.

3.2. Char and gas combustion models

For the heterogeneous char oxidation pathway, the air is portioned by constraining the available char to react in stoichiometric proportions with the available oxidizer by assuming all solid carbon oxidizes to CO_2 . The CO_2 is then allowed to dissociate into CO and O_2 at char adiabatic flame temperature of 2300 K [34]. The char oxidation products are then assumed chemically frozen as they move in thermal equilibrium with the other gases through the downstream chambers. The pyrolysis gases oxidize with the remaining air using chemical equilibrium.

4. Experimental setup and diagnostics

The test facility previously discussed in Ref. [16] is used in this study, where an Econoburn (Brocton, NY) EBW-200 wood-fired hydronic heater (WFHH) is instrumented. The setup consists of primary and secondary water circulation loops, and a heat exchanger to expel heat. The load loop contains a 300,000 BTU/hr (87.9 kW) counterflow heat exchanger to transfer heat from the boiler to a cold thermal sink. Delivered heat output (\dot{Q}_{del}) is calculated from measurements of water flow rate and boiler inlet and outlet water temperatures.

The instantaneous fuel burn rate (\dot{m}_{wood}) is measured using a fuel burn rate monitor (FBRM) [16]. The FBRM consists of a hanging basket suspended by two steel rods that run through the top of the boiler using low friction seals to prevent gas leakage. On top of the boiler, the rods are connected to a horizontal cross-member that rests on a piezoelectric-based compression load cell (Stellar Technology). The load cell is thermally insulated from the boiler to avoid biases induced by thermal gradients. Data is acquired in real-time with LabView at a frequency of 2 Hz. Air flow rate into the boiler is measured using a Bosch HFM-7 mass air flow meter, which is calibrated with an ASME standard venturi flow meter.

Two cylindrical instrument cluster cells have been designed to fit in the upper and lower port holes, (designed to measure gas temperatures and oxygen concentrations). Emissions measurements are recorded using a Testo 330-2LL gas analysis meter. Gas temperature is measured using a sheathed platinum R-type thermocouple (Omega Engineering), while oxygen in each chamber is

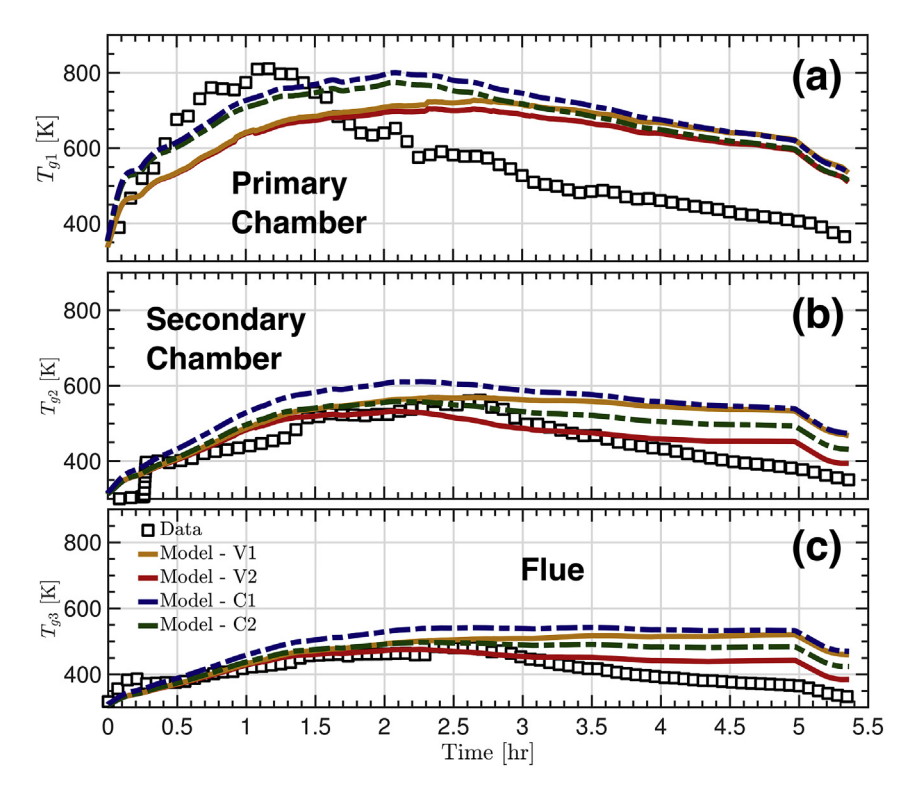


Fig. 8. Comparison of gas temperature between experimental data and lumped values from system level model.

measured using a Lambda Oxygen sensor (Bosch LSU 4.9).

5. Results and discussion

5.1. Burn rate

The fuel burn rate is shown in Fig. 6 for the wood, char, and pyrolysis gases as a function of time. Fig. 6(a) shows an increasing fuel burn rate as the wood and gases reach a local maximum at approximately 1 h, in contrast to the char burn rate where a local maximum is reached half way through the burn. Fig. 6(b) shows the char and pyrolysis gas normalized by the total wood burn rate. An identical inverse relationship to each other is seen where the production of pyrolysis gas decreases as more char is formed, consistent with the experimental observations shown in Fig. 2. After approximately 3 h the hydrogen and oxygen in the fuel has been consumed (see Fig. 4, where H/C and O/C approach zero after 3 h) and only solid carbon char remains. The trends shown in Fig. 6 further emphasize the importance in representing the gas and char separately.

5.2. Emissions

Fig. 7 shows emissions predictions versus time from the model where concentrations of O_2 in the primary, secondary, and flue chambers as well as CO_2 , H_2O and CO in the flue are compared to experimental measurements. Measurement uncertainty bounds are included with the experimental data, but in several cases may not be obvious due to the relative magnitudes of the experimental data range and the uncertainties. Four different modeling cases are presented to contrast using the constant versus variable fuel decomposition and single versus dual oxidation pathways. Cases C1 and C2 denote the constant fuel decomposition using single and dual oxidation pathways, respectively. For these cases the fuel is assumed to be red oak, $C_1H_{1.72}O_{0.72}N_{0.001}$ [35], and is consistent with preliminary energy dispersive X-ray spectroscopy (EDS)

results performed on a sample of the BIOBLOCK® fuel. Cases V1 and V2 denote the variable fuel decomposition using single and dual oxidation pathways, respectively.

5.2.1. Variable vs. constant fuel composition

Fig. 7(a), (b) and (c) show the mole fraction of oxygen within each of the three chambers compared with experimental measurements. In the primary chamber both variable fuel (V1 and V2) and constant fuel (C1 and C2) cases show comparable trends and magnitudes. Larger differences are observed in the primary chamber due to the gases being less homogenized. Better agreement to measurements is seen with V1 and V2 in the downstream chambers as the flow becomes more homogeneous, consistent with well-stirred reactor theory. The V1 and V2 trends begin to collapse with the measurements showing negligible difference in the flue where the C1 and C2 cases show an approximate peak difference of 22%.

The major species, CO_2 concentration shown in Fig. 7(d) follows a similar trend to that seen with the flue O_2 . The variable fuel cases show a negligible difference to the measurements while C1 and C2 reach a maximum difference of approximately 42%. Fig. 7(e) shows the H_2O mole fractions compared to the experimental data. The V1 and V2 cases agree with negligible differences, however, C1 and C2 follow the general trend of the wood fuel burn rate since the fuel composition does not change over time. A maximum difference of approximately 200% is seen at 2.75 h where the measured H_2O produced from the fuel reaches zero. Cases C1 and C2 continue to erroneously show water production since by definition, the elemental composition (which contains hydrogen and oxygen) remains constant throughout the burn and varies only from changes in burn rate.

5.2.2. Dual vs. single combustion pathway

The purpose of the separated pathway description is to emphasize the differences seen in the various states of the carbon

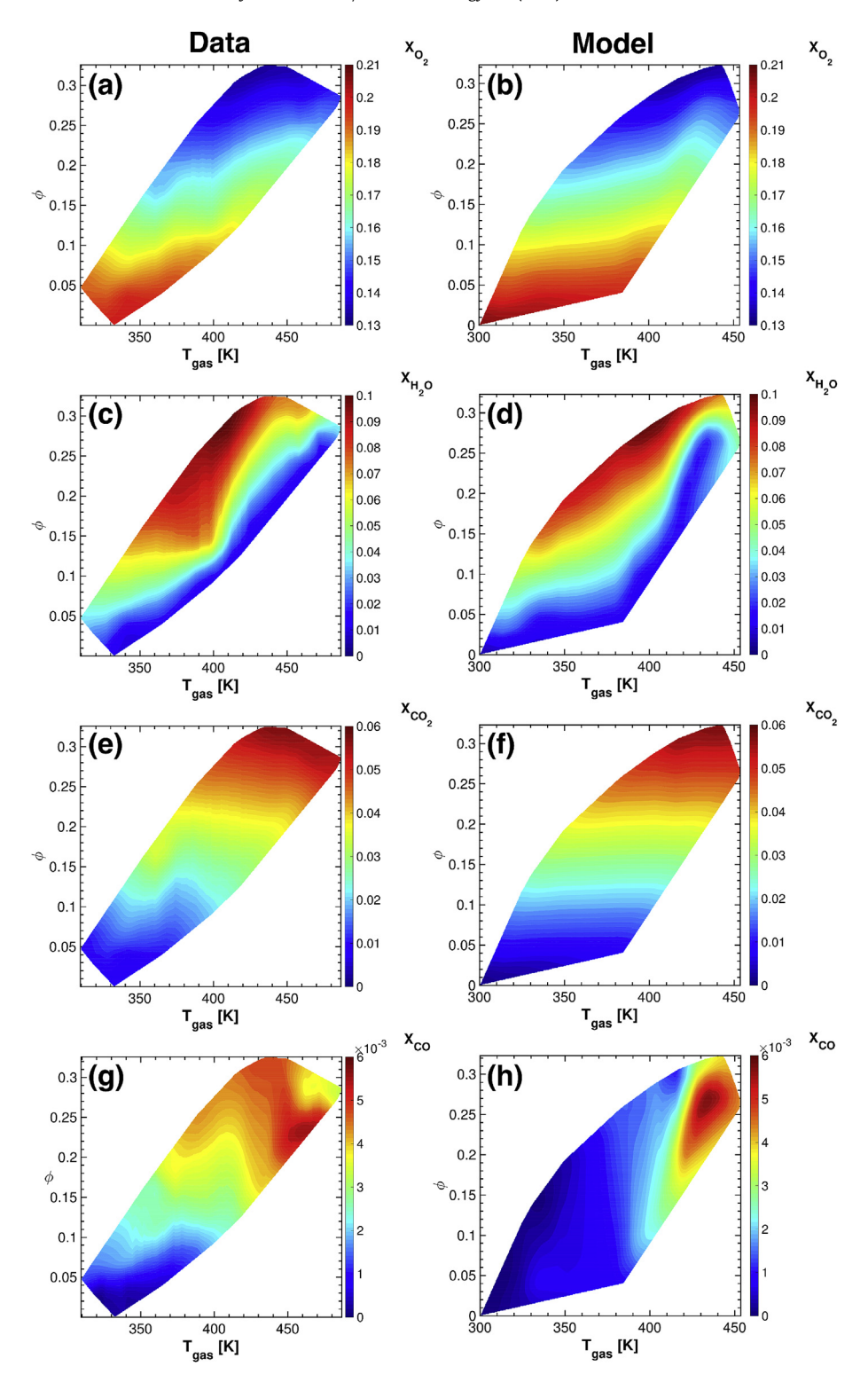


Fig. 9. Emission state maps as a function of gas temperature and equivalence ratio for major species and CO comparing experimental data to model (V2) calculations.

contained within the fuel. Therefore, differences should be most pronounced in the carbon containing minor exhaust species, *CO*. Fig. 7(f) shows the *CO* cases versus time compared to experimental measurements. Since the V1 and C1 cases show negligible *CO* emissions due to the equilibrium assumption used in the single pathway, focus will be on the dual oxidation pathway cases. The general trend shows that the C2 case (erroneously) characterizes the first *CO* peak produced primarily from the partial oxidation of

the pyrolysis gases. The V2 case is shown to characterize the second CO peak produced from the oxidation of char. The major difference is that the fuel description in the C2 case is constant and therefore is constrained to follow the trend of the total wood burn rate, effectively forcing it to agree with the first local CO peak seen in the measurements. The V2 case however, follows the trend of the char fuel burn rate and is consistent within its description of the fuel separation as well as the atomic constraints enforced by the

pyrolysis model.

5.3. Gas temperatures

Fig. 8 shows mean model gas temperatures are plotted versus time and compared to measurements using a single point bayonet thermocouple probe mounted through the chamber doors. Four model cases (V1, V2, C1 and C2) are shown with experimental measurements for each of the three main chambers. In the primary chamber the model predictions under-predict the measurements, due to the placement of the thermocouple probe within the thermally stratified chamber. Early in the burn the thermocouple is engulfed in flames from combustion of the pyrolysis gases of the full wood charge. As time evolves, the wood is consumed and reduces in height away from the thermocouple, resulting in a measured temperature that is much lower than the lumped model temperatures. As the gases further mix and are forced into the downstream chambers, the model predictions begin to show better agreement with the measurements. In particular the dual pathway cases (C2 and V2) show the best agreement with data, where the V2 case is closest due to a more accurate consideration of the fuel composition and oxidation pathways.

5.4. State maps

To better visualize the operating conditions of the boiler, three dimensional emissions maps are created, showing emissions concentrations as a function of chamber temperature and equivalence ratio (ϕ), similar to those used in the automobile industry to identify favorable combustion trajectories [36-38]. Fig. 9 show a comparison of state maps for O2, CO2, H2O, and CO comparing experimental measurements to the variable fuel dual oxidation model (V2). The comparison of magnitudes within the T- ϕ space is consistent with the time histories discussed previously in Section 5.2. Good agreement can be seen between experiment and model calculations for each O_2 (Fig. 9(a) and (b)), H_2O (Fig. 9(c) and (d)), and CO_2 (Fig. 9(e) and (f)) with some disagreement for CO (Fig. 9(g) and (h)). However, magnitudes at high temperature conditions compare well. Typically full equilibrium models with single fuel streams would expectedly produce negligible amounts of minor species CO since there is always excess O_2 to oxidize the carbon [16]. Splitting the fuel stream to account for the non-homogeneous fuel decomposition and forcing the local char surface reactions to only a limited portion of air now results in closer agreement with experimental data.

5.5. Emission index

Emission indices are often used to provide a clear expression of the amount of a particular pollutant produced per unit mass of fuel [39,40]. Fig. 10(a) shows pollutant emission per mass burned of fuel for CO and Fig. 10(b) shows CO₂. These plots show that the emissions per mass of fuel is greatly increased during the second half of a run precisely as the char oxidation process dominates. Since the emission index by definition compares the mass of a pollutant to the mass of fuel, a limiting case can be seen towards the end of the burn as the fuel is almost entirely composed of carbon char. In such a scenario, if 1 mole of fuel is to produce as much CO as possible the emission index would be limited at a maximum ratio of 28 g/mol CO to 12 g/mol C(s) or an emissions index of 2.33 (similarly for CO_2 44 g/mol CO_2 to 12 g/mol C(s) or an emission index of 3.67). Towards the end of the run as the fuel burn rate approaches zero the signal to noise ratio decreases significantly and for this reason has been truncated at 3.5 h. In general these trends are particularly informative as it provides a useful indication that the char oxidation

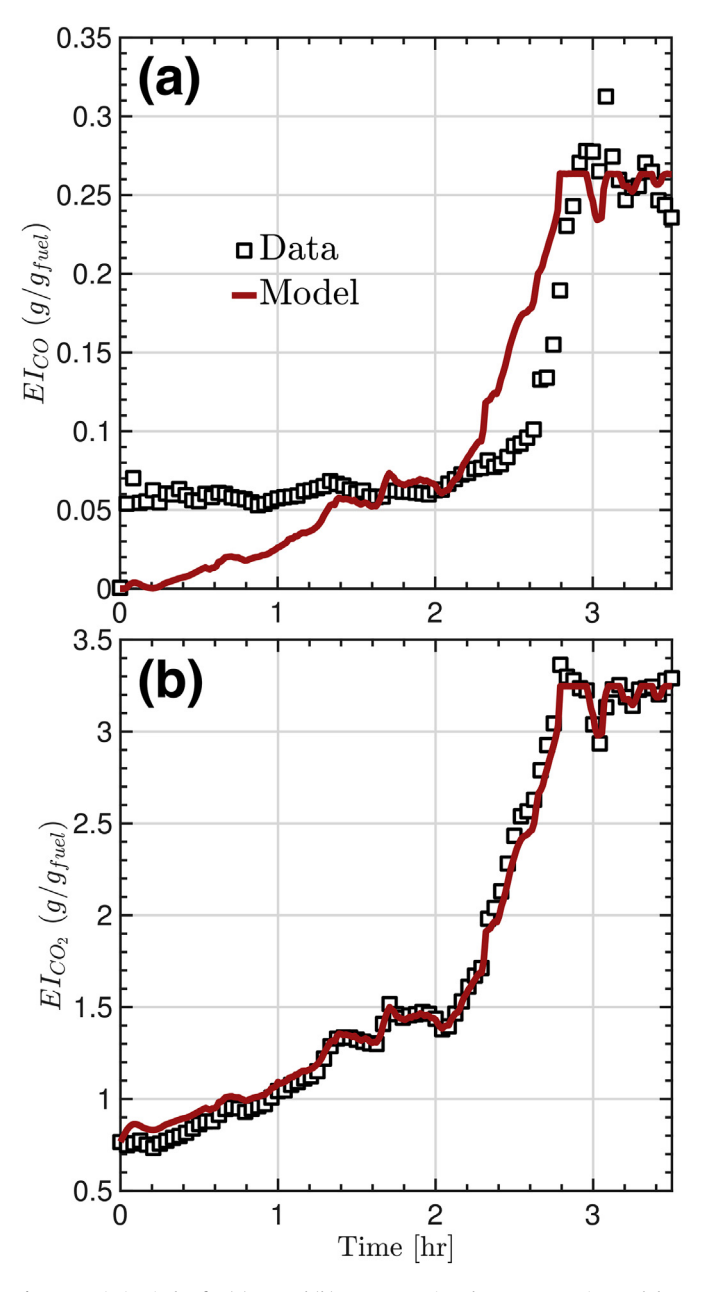


Fig. 10. Emission index for (a) CO and (b) CO_2 comparison between experimental data and model (V2) calculations.

process is responsible for increasing *CO* emissions per unit fuel by up to 400% where both the experimental measurements and model calculations agree. Additionally, the *CO* emissions index seen at the start of the burn, during the pollutant rich start up phase appears comparatively low, this is due to the majority of unbound fuel moisture being driven from the fuel, increasing the measured fuel mass. The emission indices compared to those calculated from data found in literature for a wood stove compare well to general magnitudes [41].

6. Conclusions

A three zone system level model is developed with a novel approach to predict major exhaust emissions for batch-run biomass hydronic heaters. The study demonstrates two important factors required for accurate modeling. The first is knowledge of the

transient elemental composition for the incoming fuel stream. The second is the importance of accounting for two oxidation pathways associated with pyrolysis gases and char. The indication is that the char reaction is responsible for the secondary peak often seen in batch-run CO trends. The initial peak is therefore likely due to the CO contribution from pyrolysis gas combustion which is not accurately represented by chemical equilibrium. Combination of the variable fuel and dual oxidation pathways enables a computationally low-cost system level model to accurately predict major emissions products and produce good estimates of CO emissions and chamber gas temperatures.

State map contours are created to show the path of emissions over a typical burn. Comparisons between experimental data and variable fuel dual oxidation model predictions compare very well in both trend and magnitude. Typically this level of agreement would be difficult to attain under single oxidation pathway equilibrium and constant fuel modeling approaches [16].

Finally, emissions index for CO and CO_2 comparing measured values to model predictions show that the model is capable of capturing the basic trends and magnitude for accurate characterization. The values show good agreement to those found in literature.

Acknowledgements

We thank the New York State Energy Research and Development Authority (NYSERDA) under contract number #32966 and the National Science Foundation (NSF) under grant number #1704447 for their support of this work. Thanks to Ms. Victoria Miller at Summit Wood Industries for their supply of the BIOBLOCKS® fuel used in this study also Mr. Dale Furman and Mr. Mark Odell from Econoburn for their generous donation of the EBW-200 wood fired boiler, consultation and support. We thank Mr. Xinnan Peng and the University at Buffalo Engineering Machine Shop for their support in constructing the instrument modifications to the boiler and flue.

References

- M. Guo, W. Song, J. Buhain, Bioenergy and biofuels: history, status, and perspective, Renew. Sustain. Energy Rev. 42 (2015) 712–725.
- [2] T. Butcher, N. Russell, Review of epa method 28 outdoor wood hydronic heat test results, Tech. Rep. 11–17 (2011). New York State Energy Research and Development Authority (NYSERDA).
- [3] J. Porteiro, J. Collazo, D. Patino, E. Granada, J.C. Moran Gonzalez, J.L. Míguez, Numerical modeling of a biomass pellet domestic boiler, Energy & Fuels 23 (2) (2009) 1067–1075.
- [4] M. Rabaçal, U. Fernandes, M. Costa, Combustion and emission characteristics of a domestic boiler fired with pellets of pine, industrial wood wastes and peach stones, Renew. Energy 51 (2013) 220–226.
- [5] R. Saidur, E. Abdelaziz, A. Demirbas, M. Hosszin, S. Mekhilef, A review on biomass as a fuel for boilers, Renew. Sustain. Energy Rev. 15 (2011) 2262–2289.
- [6] J. Chaney, H. Liu, J. Li, An overview of cfd modeling of small-scale fixed-bed biomass pellet boilers with preliminary results from a simplified approach, Energy Convers. Manag. 63 (2012) 149–156.
- [7] J. Collazo, J. Porteiro, J.L. Miguez, E. Granada, M. Gomez, Numerical simulation of a small-scale biomass boiler, Energy Convers. Manag. 64 (2012) 87–96.
- [8] H. Sefidari, N. Razmjoo, M. Strand, An experimental study of combustion and emissions of two types of woody biomass in a 12-mw reciprocating-grate boiler, Fuel 135 (2014) 120–129.
- [9] M. Tamura, S. Watanabe, N. Kotake, M. Hasegawa, Grinding and combustion characteristics of woody biomass for co-firing with coal in pulversized coal boilers, Fuel 134 (2014) 544–553.
- [10] J. M. Weisberger, J. P. Richter, J. C. Mollendorf, P. E. DesJardin, Predictions of non-homogeneous biomass fuel decomposition and mass loss rate using emissions measurements, in review.
- [11] M.M. Roy, K.W. Corscadden, An experimental study of combustion and emissions of biomass briquettes in a domestic wood stove, Appl. Energy 99 (2012) 206–212.

- [12] A. Ryfa, R. Buczynski, M. Chabinski, A. Szlek, R.A. Bialecki, Decoupled numerical simulation of a solid fuel fired retort boiler, Appl. Therm. Eng. 73 (2014) 794–804.
- [13] T. Persson, F. Fiedler, S. Nordlander, C. Bales, J. Paavilainen, Validation of a dynamic model for wood pellet boilers and stoves, Appl. Energy 86 (5) (2009) 645–656.
- [14] K. Jaojaruek, S. Kumar, Numerical simulation of the pyrolysis zone in a downdraft gasification process, Bioresour. Technol. 100 (23) (2009) 6052–6058
- [15] K. Jaojaruek, Mathematical model to predict temperature profile and air—fuel equivalence ratio of a downdraft gasification process, Energy Convers. Manag. 83 (2014) 223–231.
- [16] J.P. Richter, B.T. Bojko, J.C. Mollendorf, P.E. DesJardin, Measurements of fuel burn rate, emissions and thermal efficiency from a domestic two-stage woodfired hydronic heater, Renew. Energy 96 (2016) 400–409.
- [17] Z. Zhang, Y. Zhang, Y. Zhou, R. Ahmad, C. Pemberton-Pigott, H. Annegarn, R. Dong, Systematic and conceptual errors in standards and protocols for thermal performance of biomass stoves, Renew. Sustain. Energy Rev. 72 (2017) 1343–1354.
- [18] S. Sansaniwal, K. Pal, M. Rosen, S. Tyagi, Recent advances in the development of biomass gasification technology: a comprehensive review, Renew. Sustain. Energy Rev. 72 (2017) 363–384.
- [19] M. Sedighi, H. Salarian, A comprehensive review of technical aspects of biomass cookstoves, Renew. Sustain. Energy Rev. 70 (2017) 656–665.
- [20] A. Demirbas, Combustion characteristics of different biomass fuels, Prog. Energy Combust. Sci. 30 (2) (2004) 219–230.
- [21] R.P. Brent, Algorithms for Minimization without Derivatives, Courier Corporation, 2013.
- [22] J.P. Richter, J.M. Weisberger, J.C. Mollendorf, P.E. DesJardin, Emissions from a domestic two-stage wood-fired hydronic heater: effects of non-homogeneous fuel decomposition, Renew. Energy 112 (2017) 187–196.
- [23] C. Di Blasi, Modeling chemical and physical processes of wood and biomass pyrolysis, Prog. Energy Combust. Sci. 34 (1) (2008) 47–90.
- [24] C. Lautenberger, C. Fernandez-Pello, Generalized pyrolysis model for combustible solids, Fire Saf. J. 44 (6) (2009) 819–839.
- [25] M.T. McGurn, P.E. DesJardin, A.B. Dodd, Numerical simulation of expansion and charring of carbon-epoxy laminates in fire environments, Int. J. Heat Mass Tran. 55 (1–3) (2012) 272–281.
- [26] K.M. Bryden, K.W. Ragland, C.J. Rutland, Modeling thermally thick pyrolysis of wood, Biomass Bioenergy 22 (1) (2002) 41–53.
- [27] B.Y. Lattimer, J. Ouellette, Properties of composite materials for thermal analysis involving fires, Compos. Appl. Sci. Manuf. 37 (7) (2006) 1068–1081.
- [28] E. Grieco, G. Baldi, Analysis and modelling of wood pyrolysis, Chem. Eng. Sci. 66 (2011) 650–660.
- [29] T. Pattanotai, H. Watanbe, K. Okazaki, Experimental investigation of intraparticle secondary reactions of tar during wood pyrolysis, Fuel 104 (2013) 468–475.
- [30] D. Cruise, Notes on the rapid computation of chemical equilibria, J. Phys. Chem. 68 (12) (1964) 3797–3802.
- [31] D. Villars, A method of successive approximations for computing combustion equilibria on a high speed digital computer, J. Phys. Chem. 63 (4) (1959) 521–525.
- [32] W.R. Smith, R.W. Missen, Calculating complex chemical equilibria by an improved reaction-adjustment method, Can. J. Chem. Eng. 46 (4) (1968) 269–272. https://doi.org/10.1002/cjce.5450460411.
- [33] G.D. Goodwin, K.H. Moffat, L.R. Speth, Cantera: an Object-oriented Software Toolkit for Chemical Kinetics, Thermodynamics, and Transport Processes, 2017. http://www.cantera.org.
- [34] S.R. Turns, et al., An Introduction to Combustion, vol. 287, McGraw-hill, New York, 1996.
- [35] N.F.P. Agency, The SFPE Handbook of Fire Protection Engineering, National Fire Protection Agency, Quincy, MA, 1995.
- [36] T. Kamimoto, M.-h. Bae, High Combustion Temperature for the Reduction of Particulate in Diesel Engines, Tech. rep., SAE Technical Paper, 1988.
- [37] K. Akihama, Y. Takatori, K. Inagaki, S. Sasaki, A.M. Dean, Mechanism of the Smokeless Rich Diesel Combustion by Reducing Temperature, Tech. rep., SAE Technical Paper, 2001.
- [38] O. Kaario, A. Brink, K. Lehto, K. Keskinen, M. Larmi, Studying Equivalence Ratio—temperature Maps in a Heavy-duty Diesel Engine, Swedish-Finnish Flame Days Paper 16.
- [39] C.-Y. Lin, H.-A. Lin, Diesel engine performance and emission characteristics of biodiesel produced by the peroxidation process, Fuel 85 (3) (2006) 298–305.
- [40] S. Li, T. Xu, P. Sun, Q. Zhou, H. Tan, S. Hui, Nox and sox emissions of a high sulfur self-retention coal during air-staged combustion, Fuel 87 (6) (2008) 723-731.
- [41] E. Pettersson, C. Boman, R. Westerholm, D. Boström, A. Nordin, Stove performance and emission characteristics in residential wood log and pellet combustion, part 2: wood stove, Energy & Fuels 25 (1) (2011) 315–323.
- [42] R.M. Manglik, A.E. Bergles, Heat transfer and pressure drop correlations for twisted-tape inserts in isothermal tubes: Part ii—transition and turbulent flows, J. Heat Tran. 115 (4) (1993) 890—896.